Ultrasonic Measurement Models for Imaging with Phased Arrays

Lester W. Schmerr Jr.[a,b] , Brady J. Engle [a,b] , Alexander Sedov[c], and Xiongbing Li[d]

[a]*Center for NDE, Iowa State University, Ames, IA, 50011, USA*
[b]*Dept. of Aerospace Eng., Iowa State University, Ames, IA, 50011, USA*
[c]*Dept. of Mech. Eng., Lakehead University, Thunder Bay, ON, Canada P7B 5E1*
[d] *CAD/CAM Institute, Central South University, Changsha, Hunan ,410075, P.R. China*

Abstract. Ultrasonic imaging measurement models (IMMs) are developed that generate images of flaws by inversion of ultrasonic measurement models. These IMMs are generalizations of the synthetic aperture focusing technique (SAFT) and the total focusing method (TFM). A special case when the flaw is small is shown to generalize physical optics far field inverse scattering (POFFIS) images. The ultrasonic IMMs provide a rational basis for generating and understanding the ultrasonic images produced by delay-and-sum imaging methods.

Keywords: Phased Array, Synthetic Aperture Focusing Technique, Total Focusing Method, Physical Optics Far Field Inverse Scattering, Phased Array Imaging
PACS: 43.35

INTRODUCTION

With the growing use of ultrasonic phased arrays in NDE inspections, imaging has become an important tool for identifying and evaluating flaws. The synthetic aperture focusing technique (SAFT) and the total focusing method (TFM), for example, are two of the most frequently used imaging methods because of their ability to create high quality images. Both SAFT and TFM are so-called delay-and-sum methods that are based on ad-hoc procedures to form an image. However, imaging at its most fundamental level is the solution of an inverse problem so it is important to understand how the ultrasonic measurement system contributes to a flaw image through such an inversion if one wishes to extract quantitative information on the flaw from that image.

Ultrasonic measurement models have been used for over thirty years to simulate the forward problem of ultrasonic scattering, i.e. they predict how the ultrasonic voltage measured in an ultrasonic test is related to the scattering properties of a flaw, the waves generated by the interrogating transducer(s), and the electro-mechanical elements present. Since all images are formed in some fashion from these measured voltages, it is our view that one should treat the image formation process as an inversion of an ultrasonic measurement model. Here we will demonstrate that such an inversion is indeed possible using measurement models in conjunction with a strong scattering Kirchhoff approximation. This type of inversion we will call an imaging measurement model (IMM).

It will be shown that both SAFT and TFM are in fact approximate forms of our IMM approach and we will identify explicitly what part of the flaw response SAFT and TFM are trying to image. For small flaws, our IMM approach will be shown to be generalizations of a well-known inverse method called POFFIS (physical optics far field inverse scattering). Thus, our imaging measurement models will provide a foundation for understanding and quantitatively evaluating some of the most important types of imaging methods that have been developed and are currently used with ultrasonic phased array systems.

40th Annual Review of Progress in Quantitative Nondestructive Evaluation
AIP Conf. Proc. 1581, 116-123 (2014); doi: 10.1063/1.4864810

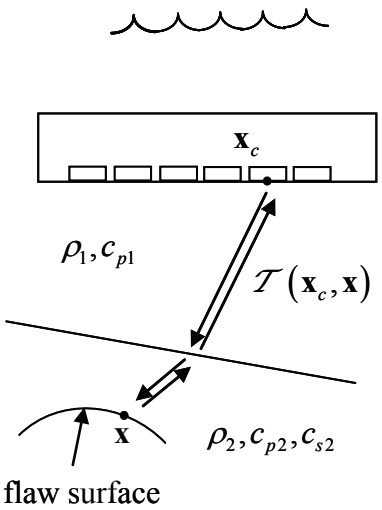

FIGURE 1. An immersion setup for imaging a flaw with the pulse-echo responses of a 2-D phased array (second dimension not shown).

PULSE-ECHO IMAGING

The SAFT imaging method was originally developed for use with single element transducers. As the transducer was scanned over a surface, the pulse-echo responses of a flaw were collected at each transducer location. The same data collection can be done with a phased array, as shown in Fig. 1. Using reciprocity relations the measured voltage from each element of the array can be simulated by a measurement model of the Auld type. For an immersion measurement, for example, we find [1]

$$V(\mathbf{x}_c,\omega)=\frac{s_I(\mathbf{x}_c,\omega)}{\rho_1 c_{p1} S\left[v(\mathbf{x}_c,\omega)\right]^2}\int_{S_f}\left(\tau_{ji}^{(1)}(\mathbf{x},\omega)v_i^{(2)}(\mathbf{x},\omega)-\tau_{ji}^{(2)}(\mathbf{x},\omega)v_i^{(1)}(\mathbf{x},\omega)\right)n_j(\mathbf{x})\,dS(\mathbf{x}). \tag{1}$$

In Eq. (1) the numbers in parentheses indicate two different states labeled (1) and (2). State (1) is the actual flaw measurement setup where the flaw is present while state (2) is where the receiving element (same as the sending element for pulse-echo measurements) acts as a transmitter instead of a receiver, and the flaw is absent. The received voltage in the frequency domain for an element whose centroid is located at $\mathbf{x}_c$ is $V(\mathbf{x}_c,\omega)$, where ω is the circular frequency. The function $s_I(\mathbf{x}_c,\omega)$ is the system function which characterizes all the electrical and electromechanical elements present in the measurement system for a given element. Since the system function may be different for different elements, we have indicated this by including $\mathbf{x}_c$ in the argument of this function. This system function can be characterized for each element in a calibration setup. Similarly, $v(\mathbf{x}_c,\omega)$ is the driving velocity on the face of the element, which is assumed to act as a piston source of sound. The quantities (ρ_1, c_{p1}) are the density and compressional wave speed of the fluid adjacent to the elements and S is the area of an element (assumed here to be the same for all elements). The fields $\left(\tau_{ij}^{(m)}(\mathbf{x},\omega), v_j^{(m)}(\mathbf{x},\omega)\right)$ $(m=1,2)$ are the stresses and velocity components on the surface, S_f, of the flaw, whose outward unit normal components are $n_j(\mathbf{x})$, for states (1) and (2). In state (1) these fields include both the incident wave fields from the element and the scattered wave fields from the flaw while in state (2) these fields are due only to the incident waves. Since measurement models like Eq. (1) can be obtained from primarily reciprocity and linearity assumptions, they are applicable in slightly

modified forms to almost all flaw measurement setups. Here, for specificity we will only use Eq. (1) which is valid for the case of immersion inspection with an array that generates bulk waves.

When the waves from an element of the array interact with a flaw, scattered waves of various types are generated. These include waves that are reflected from the front surface of the flaw (where by "front" we mean that part of the flaw that is illuminated directly by the array), flaws that reflect internally, creeping waves, etc. However, the waves that are specularly reflected from the front surface of the flaw play an especially important role since they are often the waves having the largest amplitude and hence are the most significant waves that generate an image. Thus, we will assume that it is these front surface specularly reflected waves that contribute to the measured voltage in Eq. (1). In this case, Schmerr [2] has shown that by use of the Kirchhoff approximation to model the waves that are specularly reflected from the flaw surface one can express the integrand in Eq. (1) in a much more explicit form to give

$$V(\mathbf{x}_c,\omega)=\frac{2\rho_2 c_{\beta 2} s_I(\mathbf{x}_c,\omega)}{\rho_1 c_{p1} S}\int_{S_{lit}} R^{\beta;\beta}\left[\tilde{V}_\beta(\mathbf{x}_c,\mathbf{x},\omega)\right]^2 \exp\left[2i\omega\mathcal{T}(\mathbf{x}_c,\mathbf{x})\right]dS(\mathbf{x}) \tag{2}$$

where S_{lit} is the flaw surface directly illuminated by the array, $(\rho_2, c_{\beta 2})$ are the density and wave speed (of type β where $\beta = p$ or s for incident (and scattered) compressional or shear waves, respectively), and $R^{\beta;\beta}$ is the plane wave reflection coefficient for normal incidence of a wave of type β (for both incidence and reflection) at the flaw surface. The field $\tilde{V}_\beta(\mathbf{x}_c,\mathbf{x},\omega)$ is the velocity at a point $\mathbf{x}$ on the flaw surface generated by an element located at $\mathbf{x}_c$ divided by the driving velocity, $v(\mathbf{x}_c,\omega)$ on the face of the element. This normalized velocity field can be directly calculated with ultrasonic beam models. Finally, $\mathcal{T}(\mathbf{x}_c,\mathbf{x})$ is the (one-way) travel time from an element to the point $\mathbf{x}$ on the flaw. If we now define a singular function, $\gamma_S(\mathbf{x})$, of the lit surface [3] then we can rewrite Eq. (2) as an integral over all (volumetric) space as

$$V(\mathbf{x}_c,\omega)=\frac{2\rho_2 c_{\beta 2} s_I(\mathbf{x}_c,\omega)}{\rho_1 c_{p1} S}\int_V R^{\beta;\beta}\gamma_S(\mathbf{x})\left[\tilde{V}_\beta(\mathbf{x}_c,\mathbf{x},\omega)\right]^2 \exp\left[2i\omega\mathcal{T}(\mathbf{x}_c,\mathbf{x})\right]dV(\mathbf{x}). \tag{3}$$

Equation (3) is a fundamental result since it is possible to invert this relationship to form an image of the flaw. First, we will define our flaw image, $\mathcal{I}_{\mathcal{R}}(\mathbf{x})$, as simply the singular function of the flaw surface multiplied by the plane wave reflection coefficient, i.e. $\mathcal{I}_{\mathcal{R}}(\mathbf{x}) \equiv R^{\beta;\beta}\gamma_S(\mathbf{x})$. With this definition, Eq. (3) is in a form similar to that that of a 3-D Fourier transform of the flaw image. This suggests that at least at high frequencies by performing an operation similar to an inverse Fourier transform we should be able to invert our measurement model relationship and recover the flaw image. Space does not allow us to give all the details but one can follow the steps outlined in Bleistein, Cohen and Stockwell [4] for a similar scalar problem to obtain

$$\mathcal{I}_{\mathcal{R}}(\mathbf{y})=\frac{\rho_1 c_{p1} S}{2\pi^3 \rho_2 c_{\beta 2}^4}\iint \frac{\omega^2 V(\mathbf{x}_c,\omega)}{s_I(\mathbf{x}_c,\omega)\left[\tilde{V}_\beta(\mathbf{x}_c,\mathbf{y},\omega)\right]^2}\exp\left[-2i\omega\mathcal{T}(\mathbf{x}_c,\mathbf{y})\right]d\Omega_c\, d\omega \tag{4}$$

where the integration is over a solid angle at the image point, $\mathbf{y}$, to the sending/receiving element. This integration can be transformed into one over the planar surface of the array by writing it as

$$\mathcal{I}_{\mathcal{R}}(\mathbf{y}) = \frac{\rho_1 c_{p1} S}{2\pi^3 \rho_2 c_{\beta 2}^4} \iint \frac{\omega^2 V(\mathbf{x}_c, \omega)}{s_I(\mathbf{x}_c, \omega)\left[\tilde{V}_\beta(\mathbf{x}_c, \mathbf{y}, \omega)\right]^2} \exp\left[-2i\omega \mathcal{T}(\mathbf{x}_c, \mathbf{y})\right] \frac{d\Omega_c}{dS_c} dS_c d\omega \ . \tag{5}$$

For inspection in a single medium the angle to area ratio $d\Omega_c / dS_c = \cos\beta_c / r_c^2$ where r_c is the distance from the point $\mathbf{x}_c$ on the plane of the array to an image point $\mathbf{y}$ and β_c is the angle that the ray from $\mathbf{y}$ to $\mathbf{x}_c$ makes with respect to the normal to the plane of the array. For more general inspection problems it is relatively easy to calculate this ratio via ray theory.

Equation (5) is a continuous integral form of our imaging measurement model since it assumes that both the frequency, ω, and the element location, $\mathbf{x}_c$, are continuous variables. But, it is easy to transform these integrals into the discrete sums that would be found in practice from a set of discrete elements and sampled frequencies to obtain a band and aperture limited image, $\mathcal{I}_{\mathcal{R}}^{BA}$, given by

$$\mathcal{I}_{\mathcal{R}}^{BA}(\mathbf{y}) = \frac{\Delta x_{c1} \Delta x_{c2} \Delta\omega \rho_1 c_{p1} S}{2\pi^3 \rho_2 c_{\beta 2}^4} 2\,\mathrm{Re}\left\{ \sum_{m=1}^{M} \sum_{n=1}^{L_1} \sum_{l=1}^{L_2} \omega_m^2 \frac{V(\mathbf{x}_c^{nl}, \omega_m)}{s_I(\mathbf{x}_c^{nl}, \omega_m)\left[\tilde{V}_\beta(\mathbf{x}_c^{nl}, \mathbf{y}, \omega_m)\right]^2} \cdot \frac{d\Omega_c}{dS_c}(\mathbf{x}_c^{nl}, \mathbf{y}) \exp\left[-2i\omega_m \mathcal{T}(\mathbf{x}_c^{nl}, \mathbf{y})\right] \right\}. \tag{6}$$

Here, "Re" indicates "real part of", and $(\Delta x_{c1}, \Delta x_{c2})$ are the spacing between the centroids of the array elements in the (x_1, x_2) directions, respectively, so they are just the pitches of the array in those directions. The quantity $\Delta\omega$ is the spacing of frequency components (in rad/sec).The points $\mathbf{x}_c^{nl} = (x_{c1}^{nl}, x_{c2}^{nl})$ are the discrete locations of the element centroids, ω_m are the discrete sampled frequencies, and $\mathbf{y}$ is the image point (which will also be sampled discretely in practice). The quantity $d\Omega_c / dS_c$ is the solid angle to area ratio that is calculated from each element centroid to an image point along a ray path while $\mathcal{T}(\mathbf{x}_c^{nl}, \mathbf{y})$ is the time it takes for a wave to travel from the centroid of an element to the image point. The divisions present in Eq. (6) represent a deconvolution of the measured voltage with system function and the incident wave fields. This division is reasonable to expect since one must remove these contributions from the measured voltage (contributions that are not related to the flaw) if we wish to obtain an image of flaw characteristics only. However, such deconvolution is inherently unstable in the presence of noise and so one would need to replace the straight division by an equivalent but stable process. In practice, this can be done with a Wiener filter [1], [2].

One can compare this IMM with SAFT. In the frequency domain a SAFT image, $\mathcal{I}_{SAFT}$, is given by

$$\mathcal{I}_{SAFT}(\mathbf{y}) = 2\,\mathrm{Re}\left\{ \frac{\Delta\omega}{2\pi} \sum_{m=1}^{M} \sum_{n=1}^{L_1} \sum_{l=1}^{L_2} V(\mathbf{x}_c^{nl}, \omega_m) \exp\left[-2i\omega_m \mathcal{T}(\mathbf{x}_c^{nl}, \mathbf{y})\right] \right\} \tag{7}$$

which shows that both methods are delay and sum methods but that SAFT does not compensate for system effects, incident beam effects, and other frequency and geometrical factors present in the inversion terms of the IMM.

When the flaw is small the beam correction terms in Eq. (7) can be replaced by their values at a fixed point, $\mathbf{y}_0$, near the flaw and the time term can be expressed in approximate form to first order as

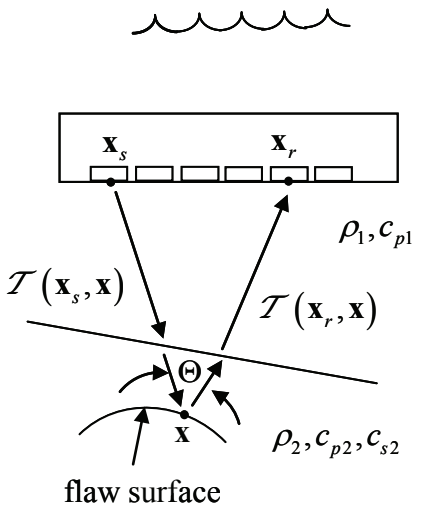

FIGURE 2. An immersion setup for imaging a flaw with the full matrix capture of all the responses of a 2-D phased array (second dimension not shown).

$\mathcal{T}(\mathbf{x}_c, \mathbf{y}) \cong \mathcal{T}(\mathbf{x}_c, \mathbf{y}_0) + \mathbf{e}_\beta \cdot (\mathbf{y} - \mathbf{y}_0) / c_{\beta 2}$, where $\mathbf{e}_\beta$ is a unit vector in the direction of propagation of the incident waves at the flaw. In this case Eq. (7) becomes

$$\mathcal{I}_{\mathcal{R}}(\mathbf{y}) = \frac{\rho_1 c_{p1} S}{2\pi^3 \rho_2 c_{\beta 2}^4} \iint \left\{ \frac{\omega^2 V(\mathbf{x}_c, \omega)}{s_I(\mathbf{x}_c, \omega)\left[\tilde{V}_\beta(\mathbf{x}_c, \mathbf{y}_0, \omega) \exp\{i\omega \mathcal{T}(\mathbf{x}_c, \mathbf{y}_0)\}\right]^2} \right.$$
$$\left. \cdot \exp\left[-2ik_{\beta 2} \mathbf{e}_\beta \cdot (\mathbf{y} - \mathbf{y}_0)\right] \frac{d\Omega_c}{dS_c} dS_c d\omega \right\}. \tag{8}$$

But in the small flaw case we can identify the combination of terms appearing in the integrand as proportional to the pulse-echo far field plane wave scattering amplitude of the flaw, $A(\mathbf{e}_\beta; -\mathbf{e}_\beta, \omega)$, giving

$$\mathcal{I}_{\mathcal{R}}(\mathbf{y}) = \frac{2}{\pi^2 c_{\beta 2}} \iint ik_{\beta 2} A(\mathbf{e}_\beta; -\mathbf{e}_\beta, \omega) \exp\left[-2i\omega \mathbf{e}_\beta \cdot (\mathbf{y} - \mathbf{y}_0)\right] \frac{d\Omega_c}{dS_c} dS_c d\omega. \tag{9}$$

Equation (9) is in a form identical to that of the scalar physical optics far field inverse scattering (POFFIS) theory of Bojarski as modified by Bleistein [3]. Engle et al. [5] show that this same result can be obtained directly by an inversion of the Thompson-Gray measurement model, which is a measurement model valid for the small flaw conditions. Thus, our pulse-echo IMM of Eq. (7) can also be thought of as a generalization of POFFIS to the case of large flaws. It is also shown in [5] through exact simulations that although the full scattering amplitude of the flaw is used to generate the flaw image, only the front surface specular response of the flaw, which is the response contained in $\mathcal{I}_{\mathcal{R}}$, is properly imaged. Other responses, such as back surface reflections and creeping waves, appear as image artifacts.

FULL MATRIX CAPTURE IMAGING

Pulse-echo responses are only a fraction of the possible sending and receiving element combinations possible with an array. In full matrix capture one collects the pitch-catch responses of all the element pairs. Using those responses in a sum and delay process similar to SAFT results in an imaging method called the total focusing method (TFM). Generally TFM is considered to result in "better" images than SAFT and because it uses all the possible response information in the array it is sometimes called the "gold standard" of imaging. However, what flaw properties are being imaged with TFM that are different from that of SAFT and what are the real quantitative improvements of TFM over SAFT? An imaging measurement model approach can answer these questions.

To form up a TFM-like image with a measurement model approach one can first consider the case where one fixed element is used as a transmitter and all the array elements are receiving. In the seismology literature this is called a fixed shot configuration. An imaging measurement model can be formed for this case in a very similar fashion to that of the pulse-echo case so we will only state the final result here, which is the pitch-catch analog of Eq. (5):

$$\mathcal{I}'_{\mathcal{R}}(\mathbf{y}) = \frac{\rho_1 c_{p1} S}{16\pi^3 \rho_2 c_{\alpha 2}^4} \iint \left| 1 + \frac{c_{\alpha 2}}{c_{\beta 2}} \cos\Theta \right| \frac{\omega^2 V(\mathbf{x}_s, \mathbf{x}_r, \omega)}{s_I(\mathbf{x}_s, \mathbf{x}_r, \omega) \tilde{V}_\beta(\mathbf{x}_s, \mathbf{y}, \omega) \tilde{V}_\alpha(\mathbf{x}_r, \mathbf{y}, \omega)} \cdot \exp\left[-i\omega \left\{ \mathcal{T}(\mathbf{x}_s, \mathbf{y}) + \mathcal{T}(\mathbf{x}_r, \mathbf{y}) \right\} \right] \frac{d\Omega_r}{dS_r} dS_r d\omega. \tag{10}$$

Here $\mathcal{I}'_{\mathcal{R}}(\mathbf{y}) \equiv R^{\alpha;\beta}(e^r_{\alpha k} n_k) \gamma_S(\mathbf{y})$ is a generalized flaw surface reflectivity where $R^{\alpha;\beta}$ is the plane wave reflection coefficient for an incident wave of type β and a reflected wave of type α and $e^r_{\alpha k} n_k = \mathbf{e}^r_\alpha \cdot \mathbf{n}$ is the cosine of the angle that the reflected wave (of type α) makes with the outward normal of the flaw. The velocity term $\tilde{V}_\beta$ is the velocity amplitude of the incident sound beam generated by the sending element divided by the driving velocity on the face of the element and $\tilde{V}_\alpha$ is the corresponding normalized velocity if the receiving element acts as a transmitter. The function $s_I(\mathbf{x}_s, \mathbf{x}_r, \omega)$ is the system function for a pair of sending and receiving elements and $\left[\mathcal{T}(\mathbf{x}_s, \mathbf{y}), \mathcal{T}(\mathbf{x}_r, \mathbf{y}) \right]$ are the travel times from the sending element and the receiving elements, respectively, to the image point, $\mathbf{y}$. The angle Θ (see Fig. 2) is the angle between the incident and scattered directions and, as in the pulse-echo case, the quantity $d\Omega_r / dS_r$ is the ratio of a solid angle to area along the scattered ray. To form up a full matrix image, one can now vary the receiving element location, $\mathbf{x}_s$, and calculate the integration of the flaw reflectivity over a solid angle as measured along the incident ray, i.e. we compute $\bar{\mathcal{I}}_{\mathcal{R}} = \int \mathcal{I}'_{\mathcal{R}} d\Omega_s$ which gives an imaging measurement in the form

$$\bar{\mathcal{I}}_{\mathcal{R}}(\mathbf{y}) = \frac{\rho_1 c_{p1} S}{16\pi^3 \rho_2 c_{\alpha 2}^4} \iiint \left| 1 + \frac{c_{\alpha 2}}{c_{\beta 2}} \cos\Theta \right| \frac{\omega^2 V(\mathbf{x}_s, \mathbf{x}_r, \omega)}{s_I(\mathbf{x}_s, \mathbf{x}_r, \omega) \tilde{V}_\beta(\mathbf{x}_s, \mathbf{y}, \omega) \tilde{V}_\alpha(\mathbf{x}_r, \mathbf{y}, \omega)} \cdot \exp\left[-i\omega \left\{ \mathcal{T}(\mathbf{x}_s, \mathbf{y}) + \mathcal{T}(\mathbf{x}_r, \mathbf{y}) \right\} \right] \frac{d\Omega_r}{dS_r} \frac{d\Omega_s}{dS_s} dS_r dS_s d\omega. \tag{11}$$

We can compare this imaging measurement model to a TFM image, written also in continuous integral form as

$$\mathcal{I}_{TFM}(\mathbf{y}) = \frac{1}{2\pi}\iiint V(\mathbf{x}_s,\mathbf{x}_r,\omega)\exp\left[-i\omega\left\{\mathcal{T}(\mathbf{x}_s,\mathbf{y})+\mathcal{T}(\mathbf{x}_r,\mathbf{y})\right\}\right]dS_r dS_s d\omega. \tag{12}$$

From Eqs. (11) and (12) we can see that the TFM, like SAFT, ignores the beam propagation and system effects so it generates a filtered version of the angular integrated front surface reflectivity of the flaw. In the study of Engle et al. [5] it is shown that the improvement in TFM over SAFT comes from the angular integration present, which eliminates artifacts like creep waves, but that other artifacts still remain in the image with the only "true" part of the image still being associated with the front surface reflectivity of the flaw.

By making the small flaw assumption one can also generate a POFFIS-style imaging measurement model for the full matrix capture case. In this case we again approximate the beam field corrections by their values at a fixed point, $\mathbf{y}_0$, near the flaw and expand the delay times to fix order as

$$\begin{aligned}\mathcal{T}(\mathbf{x}_s,\mathbf{y})+\mathcal{T}(\mathbf{x}_r,\mathbf{y}) \approx\ & \mathcal{T}(\mathbf{x}_s,\mathbf{y}_0)+\mathcal{T}(\mathbf{x}_r,\mathbf{y}_0) \\ & +\mathbf{e}_\beta^{(1)}\cdot(\mathbf{y}-\mathbf{y}_0)/c_{\beta 2}+\mathbf{e}_\alpha^{(2)}\cdot(\mathbf{y}-\mathbf{y}_0)/c_{\alpha 2}\end{aligned} \tag{13}$$

where $\left(\mathbf{e}_\beta^{(1)},\mathbf{e}_\alpha^{(2)}\right)$ are unit vectors along the incident wave directions at the flaw along ray paths from the sending and receiving element, respectively. In this case Eq. (11) becomes

$$\begin{aligned}\bar{\mathcal{I}}_{\mathcal{R}}(\mathbf{y}) = & \frac{\rho_1 c_{p1} S}{16\pi^3\rho_2 c_{\alpha 2}^4}\iiint \frac{\omega^2 V(\mathbf{x}_s,\mathbf{x}_r,\omega)}{s_I(\mathbf{x}_s,\mathbf{x}_r,\omega)\tilde{V}_\beta^{(1)}(\mathbf{x}_s,\mathbf{y}_0,\omega)\exp\left[i\omega\mathcal{T}(\mathbf{x}_s,\mathbf{y}_0)\right]} \\ & \cdot\frac{\left|1+\frac{c_{\alpha 2}}{c_{\beta 2}}\cos\Theta\right|}{\tilde{V}_\alpha^{(2)}(\mathbf{x}_r,\mathbf{y}_0,\omega)\exp\left[i\omega\mathcal{T}(\mathbf{x}_r,\mathbf{y}_0)\right]}\exp\left[-i\omega\mathbf{s}\cdot(\mathbf{y}-\mathbf{y}_0)\right]\frac{d\Omega_r}{dS_r}\frac{d\Omega_s}{dS_s}dS_r dS_s d\omega.\end{aligned} \tag{14}$$

where

$$\mathbf{s} = \mathbf{e}_\beta^{(1)}/c_{\beta 2}+\mathbf{e}_\alpha^{(2)}/c_{\alpha 2} \tag{15}$$

As in the pulse-echo case, the image can also be expressed in terms of the pitch-catch far field scattering amplitude, $A\left(\mathbf{e}_\beta^{(1)};-\mathbf{e}_\alpha^{(2)},\omega\right)$, to give

$$\begin{aligned}\bar{\mathcal{I}}_{\mathcal{R}}(\mathbf{y}) = & \frac{1}{4\pi^2 c_{\alpha 2}}\iiint (ik_{\alpha 2})\,A\left(\mathbf{e}_\beta^{(1)};-\mathbf{e}_\alpha^{(2)},\omega\right)\left|1+\frac{c_{\alpha 2}}{c_{\beta 2}}\cos\Theta\right| \\ & \cdot\exp\left[-i\omega\mathbf{s}\cdot(\mathbf{y}-\mathbf{y}_0)\right]\frac{d\Omega_r}{dS_r}\frac{d\Omega_s}{dS_s}dS_r dS_s d\omega.\end{aligned} \tag{16}$$

To our knowledge, Eq. (16) is a new imaging model of the POFFIS-type for full matrix imaging.

SUMMARY

We have developed imaging measurement models that are generalizations of both SAFT and TFM imaging and also include POFFIS-type of images as special cases. These imaging measurement models

show that SAFT is attempting to image a reflectivity defined explicitly as a reflection coefficient multiplied by a singular function that defines that flaw surface. In contrast TFM is trying to image an angular integrated form of a similar flaw surface reflectivity. It is this angular integration that allows TFM to produce "better" images than SAFT by reducing some of the artifacts and other "noise" in the imaging process. Both SAFT and TFM, however, include system and beam effects that are not flaw related and which modify the images they produce. It is also shown that POFFIS-style imaging is closely related to SAFT and TFM imaging when the incident fields do not vary significantly over the flaw surface. Thus, imaging measurement models form a rational basis for justifying and extending all of these commonly used delay-and-sum types of imaging methods.

ACKNOWLEDGMENTS

This work was supported for L.W. Schmerr and B. J. Engle by the National Science Foundation Industry/University Cooperative Research Center program at the Center for NDE, Iowa State University. A. Sedov wishes to acknowledge support by the Natural Sciences and Engineering Research Council of Canada. X. Li would like to express his gratitude to the National Natural Science Foundation of China (51005252 and 61271356) for support.

REFERENCES

1. L. W. Schmerr and S.-J. Song, Ultrasonic Nondestructive Evaluation Systems – Models and Measurements, New York, N.Y.: Springer, 2007.
2. L. W. Schmerr, Fundamentals of Ultrasonic Nondestructive Evaluation – A Modeling Approach, New York, N.Y.: Plenum Press, 1998.
3. N. Bleistein, Mathematical Methods for Wave Phenomena, New York, N.Y.: Academic Press, 1984.
4. N. Bleistein, J.K. Cohen, and J.W. Stockwell, Jr., Mathematics of Multidimensional Seismic Imaging, Migration, and Inversion, New York, N.Y.: Springer, 2000.
5. B. J. Engle, L. W. Schmerr, and A. Sedov, "Quantitative Ultrasonic Phased Array Imaging" , (this proceedings).